ACS APPLIED MATERIALS & INTERFACES

Research Article

www.acsami.org

Electron Backscatter Diffraction Study of Hexagonal Boron Nitride Growth on Cu Single-Crystal Substrates

Jennifer K. Hite,*[,†] Zachary R. Robinson,[†] Charles R. Eddy, Jr.,[†] and Boris N. Feigelson[†]

[†]U.S. Naval Research Laboratory, Washington, D.C. 20375, United States

ABSTRACT: Hexagonal boron nitride (h-BN) is an important material for the development of new 2D heterostructures. To enable this development, the relationship between crystal growth and the substrate orientation must be explored and understood. In this study, we simultaneously grew h-BN on different orientations of Cu substrates to establish the impact of substrate structure on the growth habit of thin h-BN layers. The substrates studied were a polycrystalline Cu foil, Cu(100), Cu(110), and Cu(111). Fourier transform grazing-incidence infrared reflection absorption spectroscopy (FT-IRRAS) was used to identify h-BN on copper substrates. X-ray photoelectron spectroscopy (XPS) was used to determine the effective thickness of the h-BN. Scanning electron microscopy (SEM) and electron backscatter diffraction (EBSD) were used to measure the morphology of the films and postgrowth crystal structure of the Cu substrates, respectively. Combining the SEM and EBSD images allowed for the correlation between h-BN film coverage and the crystal structure of Cu. It was found that the growth rate was inversely proportional to the surface free energy of the Cu surface, with Cu(111) having the most h-BN surface coverage. The Cu foil predominately crystallized with a (100) surface orientation, and likewise had a film coverage very close to the Cu(100).

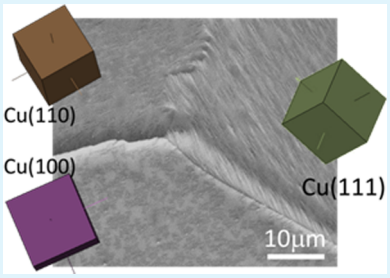

KEYWORDS: *boron nitride, 2-D, crystal orientation, EBSD, copper substrates, XPS*

INTRODUCTION

Growth of two-dimensional materials on polycrystalline Cu foil is a potential route toward commercialization of cost-effective next-generation devices. This approach was first used to grow graphene by chemical vapor deposition (CVD) on Cu foil substrates.[1] To optimize the growth process, a detailed understanding of the interaction between the two-dimensional material and underlying substrate is necessary. In the case of the heavily studied 2D material graphene, it has been shown that the surface termination of the Cu foil, which typically is (100) oriented due to plastic deformation caused by the cold rolling manufacturing process as well as recrystallization during growth, influences the growth morphology and defect density of the resulting film.[2−4] Studies of graphene on Cu(100) single-crystal substrates have shown that the surface termination impacts the rotational orientation of the films, leading to grain boundaries between rotationally misaligned domains.[5,6] Various methods have been developed to optimize graphene growth on Cu foils, including the use of Cu-enclosures,[7] oxygen predosing,[8,9] or switching to other substrate orientations, such as Cu(111).[10−12] These efforts have shown reduction in grain boundaries and rotational misalignment of graphene domains on Cu surfaces.[7−12]

In the case of hexagonal boron nitride (h-BN), similar progress in understanding the impact of the substrate on growth behavior has not yet been fully achieved. One reason for this is the difficulty associated with performing h-BN growth in an UHV environment, where in situ measurement techniques can be used. In one study, Kim et al. grew h-BN on Cu foil by sublimation of boron-containing precursors and studied the resulting films with a variety of ex situ techniques.[13] In their study, the growth of single-layer h-BN was achieved, and the crystal structure of the film was measured using selective area electron diffraction in a transmission electron microscope. These measurements showed that the h-BN films were polycrystalline, with several different rotational orientations within a relatively small (4 μm^2) area. In their study, the crystal structure of the underlying Cu foil was unclear.

In situ scanning tunneling microscopy (STM) of h-BN growth on a Cu(111) single-crystal substrate using a borazine precursor showed that h-BN grew with a variety of different rotational orientations regardless of the growth temperature.[14] For the largest-domain growth, performed at 1120 K, 13 different rotational orientations were reported, indicating a polycrystalline h-BN film. Contrasting this work, Liu et al. published a study in which single-rotational-orientation h-BN was grown on cold-rolled Cu foils, which are well-known to recrystallize with a (100) surface termination.[15] Using an atmospheric pressure growth chamber and thermal decomposition of ammonia borane as the growth precursor, μ-LEED observations showed that all of the h-BN crystallites were well-aligned to the underlying Cu(100) substrate. A study on the growth of h-BN on different orientations of Ni showed high growth rates on the (110) surfaces and very little growth on the (111) surfaces, indicating increased growth on the surface with the highest surface free energy.[16] The different results found in

Received: January 23, 2015
Accepted: June 19, 2015
Published: June 19, 2015

DOI: 10.1021/acsami.5b00723
ACS Appl. Mater. Interfaces 2015, 7, 15200−15205

each of these studies suggest a material system that is not yet fully understood.

In this work, h-BN films were grown simultaneously on polycrystalline Cu foil, Cu(111), Cu(100) and Cu(110) substrates in order to establish whether growth rates or overlayer morphology are significantly impacted by the crystal structure of the differently oriented Cu surfaces. Because Cu has a face-centered cubic crystal structure, the surface energetics can be approximated by calculating the number of missing bonds per unit area for each termination.[17] This analysis reveals that the {111} surface has the lowest surface free energy, with the {100} and {110} 15% and 22% higher, respectively.[3] Molecular dynamics were performed on Cu nanoparticles by Jia et al., which also found that Cu(111) has the lowest surface free energy, followed by Cu(100) and then Cu(110).[18] The surface free energy is expected to impact the catalytic activity of the growth surface, since atoms at a higher energy surface are expected to more readily react with the growth species. Additionally, the surface symmetry of the different crystal terminations is different, as can be seen in Table 1.

Table 1. Symmetry and Lattice Constants for Cu(111), Cu(100), Cu(110) and h-BN

	symmetry	surface lattice constant (Å)
Cu(111)	hexagonal	a_s = 2.55
Cu(100)	square	a_s = 2.55
Cu(110)	rectangular	a_s = 2.55 b_s = 3.61
h-BN	hexagonal	a_s = 2.49

EXPERIMENTAL PROCEDURES

Hexagonal boron nitride was grown simultaneously on Cu(111), Cu(100), Cu(110) and polycrystalline Cu foil substrates in a vertically oriented tube furnace. Complete details of the growth system have been previously published.[19] Polycrystalline Cu foil was purchased from Alfa Aesar (99.999%, 25 μm thick) and was plastically deformed by pressing between two hardened steel discs in a hydraulic press prior to growth. The pressing process resulted in plastic deformation of the Cu foil and has been found to increase the average grain size of the Cu foil following growth.[19] Single-crystal Cu substrates were purchased from MTI Corporation (99.9999%, 10 × 10 × 0.5 mm). All of the samples were placed inside a pyrolytic boron nitride crucible, which was mounted on a tungsten holder in the center of the furnace.

The growth conditions used for these experiments have been previously found to result in growth of separate h-BN crystallites on similarly prepared Cu foils.[19] The substrates were initially heated to a growth temperature of 930 °C in 20 sccm of hydrogen and 180 sccm of nitrogen. They were annealed at that temperature for 4 h. These anneal and growth temperatures (930 °C) were chosen because at higher temperatures the single-crystal copper samples underwent severe recrystallization. However, defects introduced to the surface by slicing and polishing of the single-crystal wafers may serve as nucleation sites for recrystallization even at these temperatures. The precursor, solid ammonia borane (BoroScience International, Inc., 99.9% pure), was sublimated at 70 °C in 840 sccm of nitrogen and 20 sccm of hydrogen, and then introduced to the growth furnace. The decomposition of ammonia borane resulted in the simultaneous release of several gaseous precursors for h-BN growth.[20] Following the 15 min growth period, the precursor was isolated from the growth furnace, and the samples were cooled in a mixture of flowing nitrogen and hydrogen.

Once the samples were cooled to room temperature, they were removed and measured by Fourier transform grazing-incidence infrared reflection absorption spectroscopy (FT-IRRAS) to verify the growth of h-BN on the copper substrates.[18] FT-IRRAS spectra were recorded using a Thermo Scientific Nicolet 8700 spectrometer combined with a Harrick Scientific Products "Focus" grazing-angle reflection accessory. The angle of incidence was 75°, and all spectra were recorded in *p*-polarization. Afterward, the samples were characterized with X-ray photoelectron spectroscopy (XPS) in a Thermo Scientific K-alpha. A monochromatic aluminum Kα (1.487 keV, 0.834 nm) X-ray source with a spot size of 400 μm was used. A LEO Supra scanning electron microscopy (SEM) instrument was used to image the surface. To examine the crystallographic orientation of the substrates after growth, an FEI Nova 600 NanoLab SEM equipped with an HKL Technology Nordlys electron backscatter diffraction (EBSD) detector was used with an 8 mm working distance, 70° tilt angle and 20 keV electron beam voltage. The EBSD patterns are formed 10−50 nm beneath the surface of each sample; as such, it is insensitive to the very thin layers of h-BN on the surface of the copper. The data gathered from this technique originates from the Cu substrate alone. Low energy electron diffraction (LEED) measurements were made using a PRI reverse-view measurement system, with an incident electron spot-size of approximately 1 mm to determine the orientation of the h-BN relative to the Cu substrates.

RESULTS AND DISCUSSION

Prior to growth, the single-crystal substrates were investigated with optical microscopy and EBSD measurements, which showed these substrates to be of a single orientation. After growth, all samples demonstrated a single FT-IRRAS peak near 820 cm^{-1}, which is attributed to the h-BN out-of-plane A_{2u} (LO) vibrational mode.[19] After the presence of h-BN on the samples was confirmed, XPS measurements were taken to measure the effective thickness of the h-BN overlayer on the Cu foil, Cu(111), Cu(100) and Cu(110) substrates. These measurements yield an effective thickness, instead of an actual thickness, as they represent an area-averaged thickness over the spot size of the measurement (~400 μm). The model used to calculate the thickness values assumes layer-by-layer growth, where the first layer completely forms before nucleation of the second layer. As that may not be the case for these films, the effective thickness instead represents the amount of h-BN. The XPS spectra can be found in Figure 1. For each of the spectra, both the B 1s and N 1s peaks corresponding to h-BN were observed. There was no evidence of satellite structure that would indicate impurity incorporation in the film. In each of the four samples, the B 1s peak was located at 190.4 eV, and the N 1s at 398.0 eV, which are close to previously reported values for B−N bonds in hexagonal BN.[21,22] Survey spectra were also measured for each sample (not shown) and indicated the presence of small amounts of oxygen and carbon, which were likely caused by sample exposure to atmospheric conditions during exchange between the growth chamber and the XPS system.

Calculation of the effective film thickness was performed by comparing the intensity from the h-BN (B 1s peak) to that of the underlying Cu (Cu 2p peak) using the following equation:

$$\frac{I_B}{I_{Cu}} = \frac{\frac{\rho_B}{M_B}\sigma_B\lambda_1\cos\theta(1 - e^{-d/\lambda_1\cos\theta})}{\frac{\rho_{Cu}}{M_{Cu}}\sigma_{Cu}\lambda_2\cos\theta(e^{-d/\lambda_3\cos\theta})} \quad (1)$$

where I_B and I_{Cu} are the areas under the B 1s and Cu $2p^{3/2}$ peaks, respectively.[23] In the numerator, ρ_B is the density of h-BN, M_B is the molecular weight of BN, σ_B is the B 1s photoionization cross section,[20] λ_1 is the effective attenuation length (EAL) of a B 1s photoelectron in h-BN, θ is the angle between the sample normal and the photoelectron detector and

DOI: 10.1021/acsami.5b00723
ACS Appl. Mater. Interfaces 2015, 7, 15200−15205

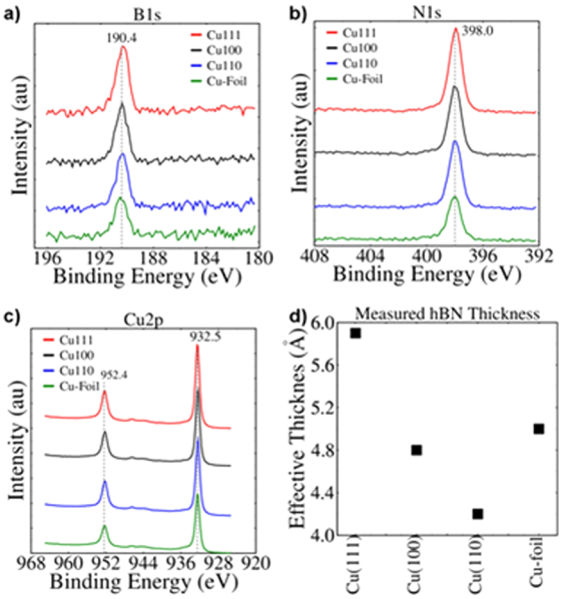

Figure 1. XPS spectra of h-BN on Cu(111), Cu(100), Cu(110) and Cu foil. The binding energies correspond to (a) B 1s, (b) N 1s, (c) Cu 2p and (d) is the calculated thickness based on eq 1.

d is the effective thickness of the h-BN films. The denominator is similar, except that λ_2 and λ_3 are the EALs of a Cu $2p^{3/2}$ photoelectron in Cu and h-BN, respectively. The EALs of the photoelectrons were calculated using the NIST EAL database.[24] Using this equation, the effective thickness of the h-BN films for several samples of different I_B/I_{Cu} ratios was solved for numerically.

The results of these calculations are plotted in Figure 1d. Growth on the Cu(111) substrate resulted in largest amount of h-BN, represented by the h-BN effective thickness of 5.9 Å. The Cu(100) and Cu foil had similar effective thicknesses h-BN, 4.8 and 5.0 Å, respectively. The Cu(110) had the least amount of growth, with 4.2 Å. Assuming an AB-stacked h-BN unit cell that is 6.6 Å thick,[25] layer number calculations equivocate these h-BN thicknesses to 0.90 layers on Cu(111), 0.75 layers on Cu foil, 0.72 layers on Cu(100) and 0.64 layers on Cu(110). This is a similar trend to FT-IRRAS data obtained on single-crystal Cu substrates.[19] Cu(111) was found to have the largest amount of h-BN on its surface, and also has the lowest surface energy of the three single crystals used. Cu(110), on the other hand, would generally be expected to have the highest catalytic activity of the three crystals used, due to its high surface energy. However, it has the least amount of h-BN on its surface. Therefore, it has been found that the growth rate of h-BN for the given growth conditions is not limited by the surface energetics of the Cu substrates.

SEM images of the sample surface were used to further study the h-BN crystallite growth morphology and coverage. In these images, crystallites of h-BN appear darker than the surrounding Cu surface, due to charging of the exposed, oxidized Cu, where the oxidation likely occurred to exposed Cu regions during transfer of the sample from the growth reactor to the SEM. At higher magnification, areas with h-BN also appear to have a rougher surface, mirroring the striated, oxide-free surface of the Cu substrates. The charging of the exposed Cu regions likely obscures the stepped surface beneath the oxide from the SEM image. The SEM images of the Cu(100), Cu(111) and Cu(110) surfaces shown in Figure 2 support the XPS findings,

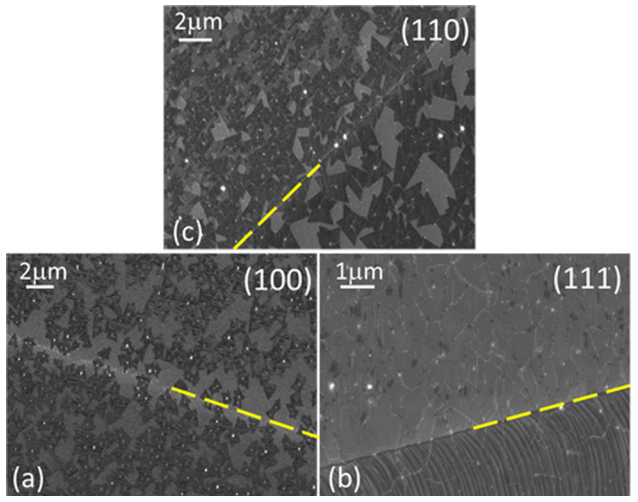

Figure 2. SEM images of h-BN growth on (a) Cu(100), (b) Cu(111) and (c) Cu(110) substrates. Dotted line shows location of Cu grain boundary. Wrinkles, indicative of complete h-BN coverage, are only observed in panel c.

with almost full coverage on the Cu(111) substrate and less coverage on the Cu(100) and Cu(110) substrates. All of these images also show grain boundaries in the substrates (dotted line), which indicate that the single crystals underwent some recrystallization during annealing and growth. Coverage on the Cu(100) and Cu(111) substrates is relatively uniform, with micrometer-scale triangular crystallites on the Cu(100) substrate and almost full coverage on the Cu(111) substrate. The lack of contrast in the Cu(111) image is due to the lack of exposed Cu-surfaces, with wrinkles over the entire surface suggesting full coverage by h-BN. These wrinkles are indicative of h-BN films and are postulated to result from differences in thermal expansion between Cu and h-BN.[13] Growth on the Cu(110) substrate varies across the surface, ranging from fully coalesced h-BN films to sporadic triangular crystallites. An example of this variable coverage on the Cu(110) substrate is illustrated in Figure 2c, where the density of crystallites is much higher in the top left grain than the bottom right grain. This suggests the possible recrystallization of the substrate during annealing and growth in the case of the Cu(110) crystal. The h-BN coverage on the Cu foil substrate (not shown) also varied, but was generally closer to that observed in the Cu(100) substrate with random triangular crystallites.

To understand further the effects of substrate and substrate grain orientation on the h-BN growth, EBSD was employed. On the Cu foil, one area that was examined showed the intersection of three different grain orientations, each of which exhibited different growth habits. The EBSD data for this area is plotted on top of the SEM image in Figure 3, with a model of the crystal orientation shown in the prevailing colors. The color legend for the Euler angles, which is the same for all EBSD maps in this paper, is shown next to the map. Above the legend is the inverse pole figure for the data, which is also color coded. Some malleability in the substrates led to surfaces with a slight curvature, which accounts for a shift in the crystallographic results. As such, the inverse pole figure can be used to determine the general crystallographic habit, but not the exact crystal indices. As most of the measurements do not extrapolate to the exact (100), (110) or (111) plane, due to slight curvature in the substrates or other defects, nomenclature in this paper will use a "(100) orientation" to mean planes close to the {100}

DOI: 10.1021/acsami.5b00723
ACS Appl. Mater. Interfaces 2015, 7, 15200−15205

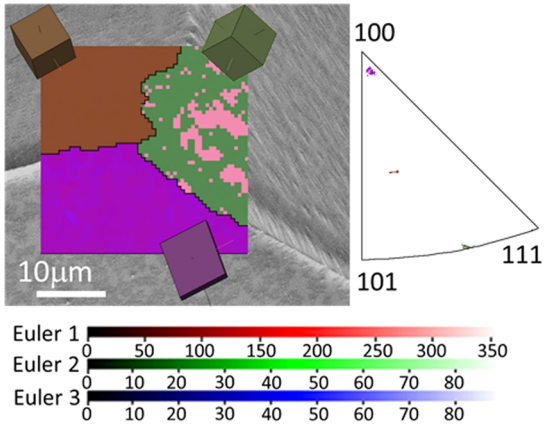

Figure 3. EBSD map imposed over SEM image of the Cu foil substrate with a model of the crystal orientation shown for each grain. Right side shows the inverse pole figure from the EBSD map. Bottom right shows color legend for Euler angles. Black line signifies grain misorientation of over 10°.

family of planes, and similar notation for (111) and (110) orientations. In the EBSD map, the lower area, displayed as purple, is (100) oriented, and shows h-BN crystallite growth. The green/pink area on the right is (111) oriented and has full coverage of h-BN, and the brown area on the left is tilted between (100) and (110) orientation and shows almost full coverage of h-BN. This figure illustrates the range of orientations and growth habits observed on the substrates. As reported elsewhere, although exhibiting grains of all types, the cold-rolled Cu foil showed a preponderance of (100) orientation,[2,3] with (111) orientation the next most prevalent orientation. The mainly (100) orientation of the Cu foil also explains the h-BN thickness correlation between the Cu foil and Cu(100) substrates from XPS calculations (Figure 1d), with similar overall growth seen on similar crystal faces.

For the single-crystal Cu substrates, the simplest case was that of the Cu(100) substrate. As shown in the EBSD map imposed over the SEM image (Figure 4), the orientation of this substrate remained (100) oriented following the growth. The inverse pole figure on the right shows that the surface is highly oriented. The h-BN on this substrate consisted of partial coverage of triangular crystallites.

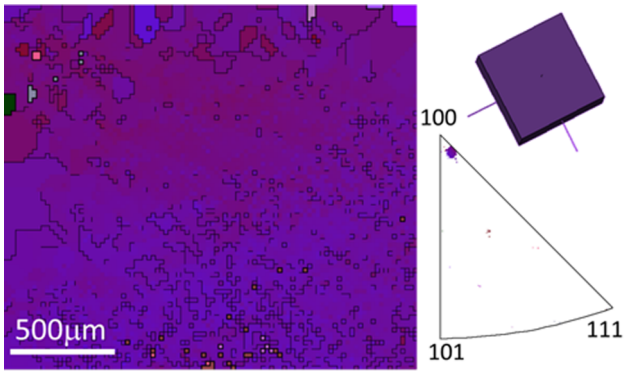

Figure 4. EBSD map of the Cu(100) substrate with a model of the crystal orientation shown on the top right. Bottom right shows the inverse pole figure from the EBSD map. Black lines indicate grain misorientation of more than 2°.

The Cu(111) substrate also underwent little recrystallization, as the (111) orientation was found in almost every region imaged, and the substrate is fully covered by h-BN. An illustration of this is shown in Figure 5, which is representative

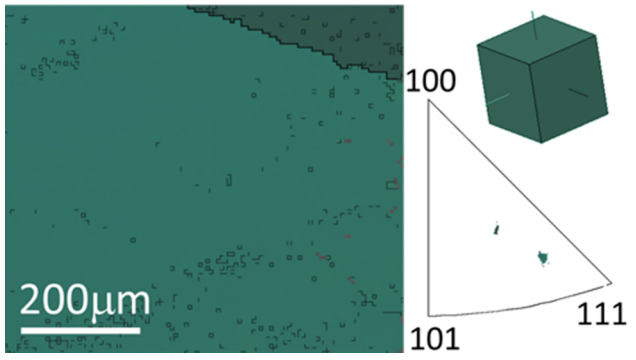

Figure 5. EBSD map of the Cu(111) substrate. Inverse pole figure and model of crystal orientation are shown to the right. This image is representative of most of the surface. Bold black lines denote grain boundaries with more than 10 degrees of misorientation, thin black lines denote those with between 2 and 10° of misorientation.

of the majority of the surface. However, a Cu(100) grain was observed (Figure 6) in one EBSD map. In contrast to the

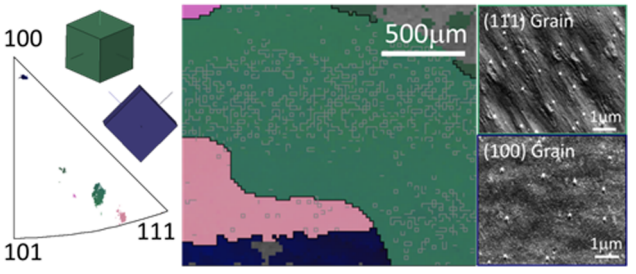

Figure 6. Middle image shows EBSD map of an area of the Cu(111) substrate with an inclusion of a (100) oriented grain. Left side shows the inverse pole figure from the EBSD map along with models of the crystal orientations in the green and navy regions. SEM images on the right show the difference in morphology between the (100) oriented grain and the rest of the (111) oriented surface. Black lines denote grain boundaries with more than 10° of misorientation.

Cu(100) oriented grains on the Cu foil or Cu(100) substrate, the Cu(100) oriented grain observed within the Cu(111) substrate exhibited the same full coverage growth behavior as the rest of the substrate, not triangular crystallites. SEM images of the two grains on the Cu(111) substrate in the insets of Figure 6 show a difference in morphology, with a cleaner surface on the (111) oriented grains and more small dots on the (100) oriented grain. From these images, it can be reasoned that the complete coverage on both grains is allowed due to the high density of dots which appear to act as nucleation sites on this Cu(100) oriented grain. This large density of nucleation sites was not observed on the Cu(100) substrate, Cu foil, or elsewhere on the Cu(111) substrate, where the nucleation site density was uniform. An alternative view is that the high growth rate on the Cu(111) surfaces allowed for overgrowth on the Cu(100) oriented grain.

For the Cu(110) substrate, the story is more complicated. As illustrated by the SEM image (Figure 2c), the varied h-BN coverage from grain to grain indicates that the substrate

DOI: 10.1021/acsami.5b00723
ACS Appl. Mater. Interfaces 2015, 7, 15200−15205

underwent significant recrystallization. This recrystallization to (111) or (100) is understood to occur due to the lowering of surface energy that is enabled when growth is performed at temperatures above copper recrystallization temperatures.[26] Defects introduced to the surface by slicing and polishing of the single-crystal wafers may serve as additional nucleation sites for recrystallization. A large-scale EBSD map of this substrate is shown in the center of Figure 7. It can be observed from the

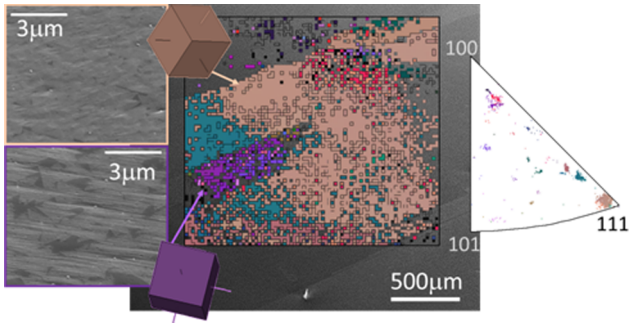

Figure 7. EBSD map of the Cu(110) surface in center. Left shows SEM images of the (100) and (111) oriented grains with models of those crystal orientations. Right shows color coordinated inverse pole figure from the EBSD map.

inverse pole figure (right side) that for this area most grains show orientations closer to the (111) or (100) orientations than the (110) orientation. The difference between the pink and green (111) oriented grains arises from in-plane orientation. In the SEM images of the (111) and (100) oriented grains (left side), the lighter, lined areas indicate h-BN growth, whereas the dark regions indicate a h-BN-free Cu surface. These two images combined with the EBSD map show that there is still more coverage of h-BN on the (111) oriented areas than on the (100) oriented ones, as was observed in the Cu foil. In other regions (not shown), the grains show orientations between the (110) and (100) orientations. These results show that growth conditions had the most drastic recrystallization effect on the Cu(110) substrate, which can be expected from the high surface energy of this orientation.

In addition to EBSD, LEED was attempted on the h-BN films to determine the rotational orientation of the h-BN with respect to the underlying substrate. The samples were loaded in the UHV system equipped with LEED, where they underwent an in situ anneal at approximately 600 °C to desorb the oxide that formed in air. Although sharp spots were seen in the LEED image, the location of (0,0) and (1,0) Cu spots could not be determined. The inability to measure LEED patterns was most likely due to the faceting that the Cu single-crystal substrates underwent during the growth. Additionally, and as discussed above, the Cu(110) single crystal underwent significant recrystallization during the growth process and was essentially polycrystalline on the surface following growth (Figure 7). Measurement of LEED patterns is extremely difficult on polycrystalline samples due to the different surface symmetries present within the measurement area.

From these results, it can be concluded that the close lattice match between the Cu(111) and h-BN facilitate the growth of h-BN films, regardless of the low surface energy, as growth on these faces resulted in the thickest and most coalesced films via XPS measurements and SEM observations, respectively. Although growth on the (100) and (110) orientations still occurs, it does so at a slower rate than on the Cu(111) surfaces. Cu(110), on the other hand, would generally be expected to have the highest catalytic activity of the three crystals used, due to its high surface energy. However, it has the least amount of h-BN on its surface. Therefore, it has been found that the growth rate of h-BN for the given growth conditions is not limited by the surface energetics of the Cu substrates, unlike the growth of h-BN on Ni reported by Lee et al.[16] These conclusions are consistent with theoretical results for h-BN monolayers on the (111) surfaces of a range of fcc metals, which show that the strain energy in the BN layer increases with the degree of lattice mismatch between h-BN and the substrate.[27] This variation of thickness with Cu crystal orientation are also consistent with FT-IRRAS studies.[19]

SUMMARY

In conclusion, the growth habits of h-BN on Cu foil and single-crystal oriented Cu substrates were studied via XPS, SEM and EBSD. XPS determined the average growth of h-BN was thickest on the Cu(111) substrate. By combining these XPS results with EBSD and SEM images of growth on the different crystal orientations, it was shown that h-BN growth is most rapid on the Cu(111) surfaces and slower on the two other orientations studied, with Cu(110) being the slowest growth surface. These conclusions show that the growth rate of h-BN is inversely proportional to the Cu surface energy.

AUTHOR INFORMATION

Corresponding Author

*J. K. Hite. E-mail: jennifer.hite@nrl.navy.mil.

Notes

The authors declare no competing financial interest.

ACKNOWLEDGMENTS

Work at the U.S. Naval Research Laboratory is supported by the Office of Naval Research. Z.R.R. thanks ASEE for postdoctoral support.

REFERENCES

(1) Li, X.; Cai, W.; An, J.; Kim, S.; Nah, J.; Yang, D.; Piner, R.; Velamakanni, A.; Jung, I.; Tutuc, E.; Banerjee, S. K.; Colombo, L.; Ruoff, R. S. Large-Area Synthesis of High-Quality and Uniform Graphene Films on Copper Foils. *Science* **2009**, *324*, 1312−1314.

(2) Wood, J. D.; Schmucker, S. W.; Lyons, A. S.; Pop, E.; Lyding, J. W. Effects of Polycrystalline Cu Substrate on Graphene Growth by Chemical Vapor Deposition. *Nano Lett.* **2011**, *11*, 4547−4554.

(3) Robinson, Z. R.; Tyagi, P.; Murray, T. M.; Ventrice, C. A., Jr.; Chen, S.; Munson, A.; Magnuson, C. W.; Ruoff, R. S. Substrate Grain Size and Orientation of Cu and Cu−Ni Foils Used for the Growth of Graphene Films. *J. Vac. Sci. Technol., A* **2012**, *30*, 011401.

(4) Rasool, H. I.; Song, E. B.; Mecklenburg, M.; Regan, B. C.; Wang, K. L.; Weiller, B. H.; Gimzewski, J. K. Atomic-Scale Characterization of Graphene Grown on Copper (100) Single Crystals. *J. Am. Chem. Soc.* **2011**, *133*, 12536−12543.

(5) Yuan, Q.; Song, G.; Sun, D.; Ding, F. Formation of Graphene Grain Boundaries on Cu(100) Surface and a Route towards Their Elimination in Chemical Vapor Deposition Growth. *Sci. Rep.* **2014**, *4*, 6541.

(6) Kim, K.; Lee, Z.; Regan, W.; Kisielowski, C.; Crommie, M. F.; Zettl, A. Grain Boundary Mapping in Polycrystalline Graphene. *ACS Nano* **2011**, *5*, 2142−2146.

(7) Li, X.; Magnuson, C. W.; Venugopal, A.; Tromp, R. M.; Hannon, J. B.; Vogel, E. M.; Colombo, L.; Ruoff, R. S. Large-Area Graphene

DOI: 10.1021/acsami.5b00723
ACS Appl. Mater. Interfaces 2015, 7, 15200−15205

Single Crystals Grown by Low-Pressure Chemical Vapor Deposition of Methane on Copper. *J. Am. Chem. Soc.* **2011**, *133*, 2816−2819.
(8) Hao, Y.; Bharathi, M. S.; Ruoff, R. S. The Role of Surface Oxygen in the Growth of Large Single-Crystal Graphene on Copper. *Science* **2013**, *342*, 720−723.
(9) Robinson, Z. R.; Ong, E. W.; Mowll, T. R.; Tyagi, P.; Gaskill, D. K.; Geisler, H.; Ventrice, C. A. Influence of Chemisorbed Oxygen on the Growth of Graphene on Cu(100) by Chemical Vapor Deposition. *J. Phys. Chem. C* **2013**, *117*, 23919−23927.
(10) Robinson, Z. R.; Tyagi, P.; Mowll, T. R.; Ventrice, C. A., Jr.; Hannon, J. B. Argon-Assisted Growth of Epitaxial Graphene on Cu(111). *Phys. Rev. B* **2012**, *86*, 235413.
(11) Hu, B.; Ago, H.; Ito, Y.; Kawahara, K.; Tsuji, M.; Magome, E.; Sumitani, K.; Mizuta, M.; Ikeda, K.; Mizuno, S. Epitaxial Growth of Large-Area Single-Layer Graphene Over Cu(111)/Sapphire by Atmospheric Pressure CVD. *Carbon* **2012**, *50*, 57−65.
(12) Ago, H.; Kawahara, K.; Ogawa, Y.; Tanoue, S.; Bissett, M. A.; Tsuji, M.; Sakaguchi, H.; Koch, R. J.; Fromm, F.; Seyller, T.; et al. Epitaxial Growth and Electronic Properties of Large Hexagonal Graphene Domains on Cu(111) Thin Film. *Appl. Phys. Express* **2013**, *6*, 075101.
(13) Kim, K. K.; Hsu, A.; Jia, X.; Kim, S. M.; Shi, Y.; Hofmann, M.; Nezich, D.; Rodriguez-Nieva, J. F.; Dresselhaus, M.; Palacios, T.; et al. Synthesis of Monolayer Hexagonal Boron Nitride on Cu Foil Using Chemical Vapor Deposition. *Nano Lett.* **2012**, *12*, 161−166.
(14) Joshi, S.; Ecija, D.; Koitz, R.; Iannuzzi, M.; Seitsonen, A. P.; Hutter, J.; Sachdev, H.; Vijayaraghavan, S.; Bischoff, F.; Seufert, K.; Barth, J. V.; Auwarter, W. Boron Nitride on Cu(111): An Electronically Corrugated Monolayer. *Nano Lett.* **2012**, *12*, 5821−5828.
(15) Liu, Z.; Song, L.; Zhao, S.; Huang, J.; Ma, L.; Zhang, J.; Lou, J.; Ajayan, P. M. Direct Growth of Graphene/Hexagonal Boron Nitride Stacked Layers. *Nano Lett.* **2011**, *11*, 2032−2037.
(16) Lee, Y. H.; Liu, K. K.; Lu, A. Y.; Wu, C. Y.; Lin, C. T.; Zhang, W.; Su, C. Y.; Hsu, C. L.; Lin, T. W.; Wei, K. H.; Shi, Y.; Li, L. J. Growth Selectively of Hexagonal-Boron Nitride Layers on Ni with Various Crystal Orientations. *RSC Adv.* **2012**, *2*, 111−115.
(17) Ibach, H. *Physics of Surfaces and Interfaces*; Springer: New York, NY, 2006.
(18) Jia, M.; Lai, Y.; Tian, Z.; Liu, Y. Calculation of the Surface Free Energy of fcc Copper. *Modell. Simul. Mater. Sci. Eng.* **2009**, *17*, 015006.
(19) Feigelson, B. N.; Bermudez, V. M.; Hite, J. K.; Robinson, Z. R.; Wheeler, V. D.; Sridhara, K.; Hernandez, S. Growth and Spectroscopic Characterization of Monolayer and Few-Layer Hexagonal Boron Nitride on Metal Substrates. *Nanoscale* **2015**, *7*, 3694−3702.
(20) Wolf, G.; Baumann, J.; Baitalow, F.; Hoffmann, F. P. Calorimetric Process Monitoring of Thermal Decomposition of B−N−H Compounds. *Thermochim. Acta* **2000**, *343*, 19−25.
(21) Moulder, J. F.; Stickle, W. F.; Sobol, P. E.; Bombem, D. *Handbook of X-ray Photoelectron Spectroscopy*; Perkin Elmer Co.: Eden Praire, MN, 1992.
(22) Song, L.; Ci, L.; Lu, H.; Sorokin, P. B.; Jin, C.; Ni, J.; Kvashnin, A. G.; Kvashnin, D. G.; Lou, J.; Yakobson, B.; Ajayan, P. M. Large Scale Growth and Characterization of Atomic Hexagonal Boron Nitride Layers. *Nano Lett.* **2010**, *10*, 3209−3215.
(23) *Electron Spectroscopy: Theory, Techniques and Applications*; Brundle, C. R., Baker, A. D., Eds.; Vol. *1*−*3*; Academic Press: New York, NY, 1977−1979.
(24) Jablonski, A.; Powell, C. J. *NIST Effective-Attenuation-Length Database*, Version 1.3; National Institute of Standards and Technology: Gaithersburg, MD, 2011.
(25) Pease, R. S. An X-ray Study of Boron Nitride. *Acta Crystallogr.* **1952**, *5*, 356−361.
(26) Field, D. P.; Bradford, L. T.; Nowell, M. M.; Lillo, T. M. The Role of Annealing Twins During Recrystallization of Cu. *Acta Mater.* **2007**, *55*, 4233−4241.
(27) Laskowski, R.; Blaha, P.; Schwarz, K. Bonding of Hexagonal BN to Transition Metal Surfaces: An ab Initio Density-Functional Theory Study. *Phys. Rev. B* **2008**, *78*, 045409.

DOI: 10.1021/acsami.5b00723
ACS Appl. Mater. Interfaces 2015, 7, 15200−15205